

Optimal quantum transport on a ring via locally monitored chiral quantum walks

Sara Finocchiaro,^{1,2} Giovanni Luilli,³ Giuliano Benenti,^{1,2} Matteo G.A. Paris,^{3,2} and Luca Razzoli^{1,2,*}

¹*Center for Nonlinear and Complex Systems, Dipartimento di Scienza e Alta Tecnologia,
Università degli Studi dell'Insubria, Via Valleggio 11, 22100 Como, Italy*

²*Istituto Nazionale di Fisica Nucleare, Sezione di Milano, I-20133 Milano, Italy*

³*Dipartimento di Fisica, Università di Milano, I-20133 Milan, Italy*

(Dated: July 16, 2025)

In purely coherent transport on finite networks, destructive interference can significantly suppress transfer probabilities, which can only reach high values through careful fine-tuning of the evolution time or tailored initial-state preparations. We address this issue by investigating excitation transfer on a ring, modeling it as a locally monitored continuous-time chiral quantum walk. Chirality, introduced through time-reversal symmetry breaking, imparts a directional bias to the coherent dynamics and can lift dark states. Local monitoring, implemented via stroboscopic projective measurements at the target site, provides a practical detection protocol without requiring fine-tuning of the evolution time. By analyzing the interplay between chirality and measurement frequency, we identify optimal conditions for maximizing the asymptotic detection probability. The optimization of this transfer protocol relies on the spectral properties of the Perron-Frobenius operator, which capture the asymptotic non-unitary dynamics, and on the analysis of dark states. Our approach offers a general framework for enhancing quantum transport in monitored systems.

I. INTRODUCTION

In a *classical random walk* the walker takes steps in random directions through a network, resulting in diffusive spreading. In a *quantum walk*, instead, the walker takes a quantum superposition of paths, leading to quantum interference effects [1, 2]. While constructive interference enables ballistic spreading (faster than the classical diffusive spreading), destructive interference can hinder transport or cause localization [3].

Continuous-time quantum walks are versatile for modeling coherent transport in discrete systems [4]. Equivalent to the tight-binding approximation in solid-state physics and in Hückel's molecular-orbital theory, their applicability is broad across systems, ranging from solid-state to biological ones [5–11]. In recent decades, several studies on environment-assisted quantum transport have highlighted the beneficial interplay of coherent and incoherent dynamics [12–16], where the loss of phase coherence, e.g., due to dephasing, can enhance transport by suppressing destructive interference [17, 18]. Focusing on purely coherent transport, achieving unit transport efficiency in highly symmetric networks often requires non-trivial delocalized initial states due to symmetry-protected states [19, 20]. Breaking some symmetries, e.g., via network defects [21, 22], can improve transport.

Chiral quantum walks leverage time-reversal symmetry breaking, typically through complex-valued edge weights [23, 24], to enable controlled directional transport [25–27] or its suppression [28], with promising applications in routing [29]. While chirality can mitigate destructive interference by affecting phase coherences, achieving nearly

optimal transfer—even on a simple ring [26]—often requires fine control of the evolution time [30]. This represents an experimental challenge, as it requires a priori knowledge of the optimal time to halt the transfer protocol. Classically, this relates to first-passage-time problems [31–34], which address the statistics of the time a random walker takes to reach a target. However, in a quantum context the concept of first passage is not meaningful; instead, measurements must be explicitly incorporated [19], leading to the notion of first-*detected*-passage time [35–39]. The latter bridges unitary dynamics and measurement-induced collapse in monitored systems [40], offering insights into quantum-classical transition and measurement back-action.

While it is known that chirality can mitigate destructive interference by lifting energy degeneracies, associated to *dark states* that prevent detection for certain initial conditions [38, 41, 42], the optimal interplay between chirality and measurement frequency has yet to be explored. In this work, we address this gap by investigating a monitored chiral quantum walk on a ring (see Fig. 1), where the purely coherent evolution of the system is repeatedly interrupted by projective measurements at the target. We show how to leverage chirality and detection period to significantly enhance transport. Specifically, we derive a general prescription for maximizing the asymptotic detection probability, relying on the Perron-Frobenius spectrum of the non-unitary dynamics and on the analysis of dark states.

The paper is organized as follows: In Section II, we introduce the chiral system under investigation and briefly review the first-detected-passage time problem. In Section III we present results about the maximization of the detection probability. Relying on the analysis of the Perron-Frobenius spectrum and dark states, in Section IV we discuss the optimal conditions for excitation transfer in the long-time limit and draw conclusions in Section

* Currently at Dipartimento di Fisica “Alessandro Volta”, Università degli Studi di Pavia, Via Bassi 6, 27100 Pavia, Italy; INFN, Sezione di Pavia, Via Bassi 6, 27100 Pavia, Italy.

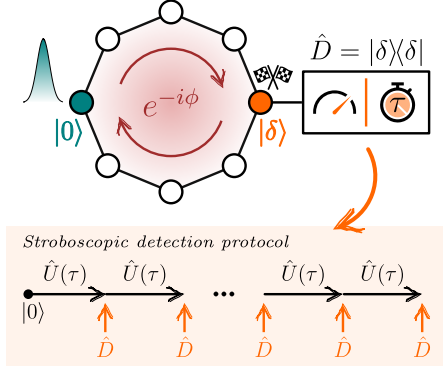


FIG. 1. Schematic illustration of the excitation transfer, modeled as a locally monitored chiral quantum walk under a stroboscopic detection protocol, investigated in this work.

V.

II. FIRST-DETECTED-PASSAGE-TIME PROBLEM

Within the framework of first-detected-passage-time problems, our purpose is to investigate coherent excitation transfer on a ring—a cycle graph with finite number of sites N —under local monitoring. We model the transfer as a continuous-time chiral quantum walk, and assume stroboscopic detection for local monitoring (see Fig. 1). For this system, a convenient basis of the Hilbert space is represented by the localized states on the sites of the graph, $\{|j\rangle\}_{j=0,\dots,N-1}$. In such a basis, the Hamiltonian of the chiral quantum walk can be written as [25]

$$H = \sum_{j=0}^{N-1} e^{-i\phi} |(j+1)_N\rangle\langle j| + e^{i\phi} |(j-1)_N\rangle\langle j| \quad (1)$$

where $(j \pm 1)_N = (j \pm 1) \bmod N$ due to the periodic boundary conditions. We set all the diagonal elements to zero to solely focus on the effects of the phase $\phi \in [-\frac{\pi}{N}, \frac{\pi}{N}]$ responsible for the chirality. The upper bound follows from the fact that, in loops, the overall net phase is what matters, and so $-\pi \leq N\phi \leq \pi$ [26, 43]. Eigenvectors and eigenvalues of the Hamiltonian (1), a circulant matrix, respectively read

$$|\lambda_j\rangle = \frac{1}{\sqrt{N}} \sum_{k=0}^{N-1} e^{i\frac{2\pi}{N}jk} |k\rangle, \quad (2)$$

$$\lambda_j = 2 \cos\left(\phi - \frac{2\pi}{N}j\right), \quad (3)$$

with $j = 0, \dots, N-1$. Under the time-independent Hamiltonian (1), the system initially prepared in a state $|\psi_0\rangle \equiv |\psi(t=0)\rangle$ evolves unitarily according to

$$|\psi(t)\rangle = \hat{U}(t) |\psi_0\rangle = e^{-iHt} |\psi_0\rangle, \quad (4)$$

where we set $\hbar = 1$.

In quantum systems the *first-detected-passage time*, or *hitting time*, is defined through repeated monitoring at the target site [19, 37], where the detector reveals the presence or absence of the walker. We assume a stroboscopic detection protocol in which projective measurements are performed at times $\tau, 2\tau, 3\tau, \dots$, where the arbitrary finite sampling period $\tau > 0$ is chosen by the experimentalist. The scheme is illustrated in the box in Fig. 1: starting from an initial state $|\psi_0\rangle = |0\rangle$ localized at site (without loss of generality we assume the 0th), the monitored dynamics alternates unitary evolution, $\hat{U}(\tau)$ (4), and projective measurements at the target site, $\hat{D} = |\delta\rangle\langle\delta|$. In the following, we assume the target site to be the opposite to the initial one, i.e., $|\delta\rangle = |N/2\rangle$ for even N , and $|\delta\rangle = |(N \pm 1)/2\rangle$ for odd N . A typical run of the monitored dynamics produces a string of binary measurement outcomes: a sequence of *no* (the walker has not been detected) repeated until a *yes* (the walker has been detected) occurs at time $n\tau$, i.e., at the n th detection attempt. This time $n\tau$ is then defined as the first-detected-passage time for the run under investigation. The probability F_n to first detect the walker at the n th attempt is [37]

$$F_n = \langle \theta_n | \hat{D} | \theta_n \rangle, \quad (5)$$

where

$$|\theta_n\rangle = U(\tau)[(\mathbb{I} - \hat{D})U(\tau)]^{n-1} |\psi_0\rangle, \quad (6)$$

is the first-detection (unnormalized) vector. The detection probability up to time $n\tau$ is

$$P_{\text{det}}(n) = \sum_{m=1}^n F_m. \quad (7)$$

As a final remark, we point out that we investigate local monitoring for excitation transfer since purely-coherent transport performs poorly. Indeed, under unitary dynamics, the transfer probability $P_\delta(t) = |\langle \delta | \hat{U}(t) | \psi_0 \rangle|^2$ typically exhibits low values with rare sharp peaks (see Appendix A). By leveraging chirality, ϕ , and local monitoring, τ , we aim at finding a robust optimal transfer protocol, meaning that no fine-tuning of parameters is required to achieve sufficiently high values of detection probability.

III. MAXIMIZATION OF THE DETECTION PROBABILITY

In this section, we aim at maximizing the detection probability (7) over the key parameters of our model: the detection period τ between consecutive measurements, and the phase ϕ in the Hamiltonian (1). This optimization is subject to a constraint, as we assume the total time T of the process to be a finite resource. Therefore, what we maximize is the detection probability $P_{\text{det}}(\phi, \tau)$

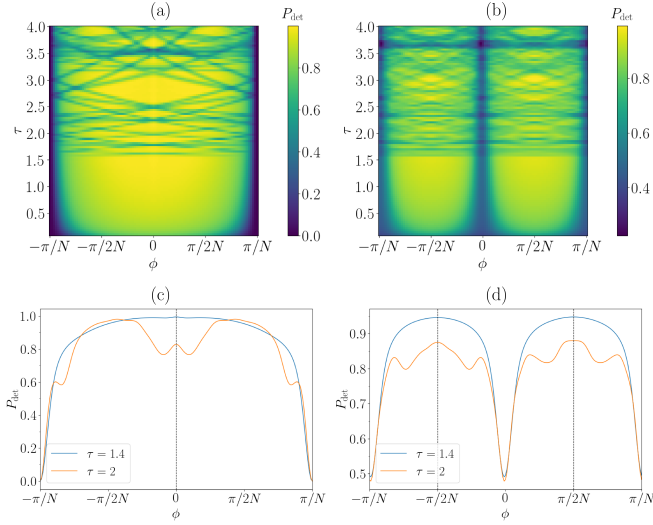


FIG. 2. Detection probability as a function of the phase ϕ and the sampling period τ at fixed total observation time $T = 200$. Density plots $P_{\text{det}}(\phi, \tau)$ (a) for $N = 20$ and $\delta = N/2$ and (b) for $N = 21$ and $\delta = (N-1)/2$. (c,d) Curves $P_{\text{det}}(\phi)$ at given τ for system size N and detection site δ as in (a,b), respectively.

after n detection attempts, where $n = \lfloor T/\tau \rfloor$. Therefore, the detection probability we discuss is upper bounded by its asymptotic value, $P_{\text{det}}(\phi, \tau) \leq P_{\text{det}}(n \rightarrow \infty)$. In the following, we conveniently set $T = 200$, a value which allows us to achieve detection probabilities $> 90\%$ when the number of sites N is relatively small (see Section IV C), while keeping the number of measurements n limited. In the next sections, we will focus first on the role of the phase ϕ , and then on that of the period τ .

A. Optimal phase ϕ

To get a first insight on how the detection probability depends on the parameters of interest, in Fig. 2 we show the density plots of $P_{\text{det}}(\phi, \tau)$ for a fixed number of sites, distinguishing between even $N = 20$ and odd $N = 21$. For even N [Fig. 2(a)], we observe that for $\tau < \tau^*$ the detection probability is maximized at $\phi = 0$, decreases as $|\phi|$ increases, and vanishes at $\phi = \pm\pi/N$. Above this threshold $\tau^* \approx 1.55$ on the detection interval (see Section IV B), complex patterns emerge. Therefore, introducing a nonzero phase in the Hamiltonian (chirality) hinders excitation transfer between opposite sites of the symmetric cycle (even N), as it reduces the detection probability at the target. In contrast, chirality enhances this transfer in the asymmetric cycle (odd N) [Fig. 2(b)]. The directionality induced by the nonzero phases causes the detection probability to increase at either of the two target sites $\delta = (N \pm 1)/2$ opposite to the starting one. In particular, for $\tau < \tau^*$ the detection probability is always maximized at $\phi_{\text{opt}} = \pm\pi/2N$, and minimized at $\phi = 0, \pm\pi/N$. As a final remark, we point that while

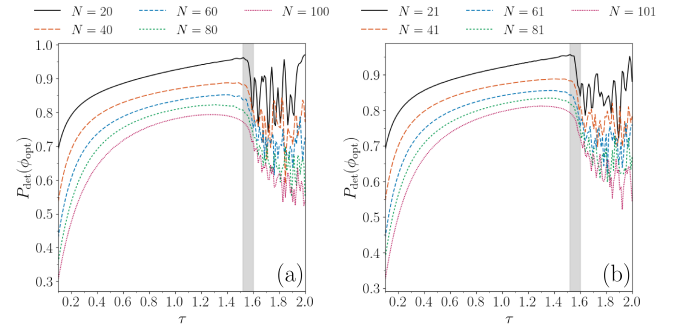


FIG. 3. Detection probability as a function of τ evaluated at fixed $\phi = \phi_{\text{opt}}$ and $T = 200$ for various N . (a) Even N with $\delta = N/2$ and $\phi_{\text{opt}} = 0$. (b) Odd N with $\delta = (N-1)/2$ and $\phi_{\text{opt}} = \pi/2N$. For each N , a threshold τ^* can be identified within a relatively narrow region (grey-shaded).

$P_{\text{det}}(\phi, \tau) = P_{\text{det}}(-\phi, \tau)$ for even N , this symmetry is lifted for odd N [Fig. 2(c,d)]. However, for odd N the detection probability is symmetric upon changing both the target site *and* the sign of ϕ .

B. Optimal measurement period τ

The detection period τ plays a crucial role, as the detection probability for both even and odd N shows two qualitatively distinct regimes separated by a sharp transition at a critical threshold τ^* [see Fig. 2(a,b)]. When $\tau < \tau^*$, $P_{\text{det}}(\phi, \tau)$ is smooth, generally increasing with τ (recall we fixed $T = n\tau$), and remains high over extended intervals. Conversely, when $\tau > \tau^*$, a highly structured pattern with sharp oscillations emerges. As $\tau \rightarrow 0$, we observe a quantum Zeno effect [44, 45]. Here, frequent measurements performed on a state $|\delta\rangle$ (orthogonal to the initial one) effectively confine the walker's evolution in the subspace orthogonal to the detection subspace, preventing it from reaching $|\delta\rangle$. As a result, the detection probability approaches zero as $\tau \rightarrow 0$. A qualitatively analogous behavior is observed when varying the number of sites N , with the critical threshold τ^* exhibiting only minor variation. This is illustrated in Fig. 3, where $P_{\text{det}}(\phi_{\text{opt}}, \tau)$ is plotted for different N . As evident from Figs. 2-3, although maxima of the detection probability also occur in the region $\tau > \tau^*$, attaining them would require a fine tuning of τ that is difficult to achieve in practice. Since we are interested in a robust protocol, we maximize the detection probability in the relatively wide region $\tau < \tau^*$.

IV. ANALYSIS AND DISCUSSION

In this section, we offer two complementary interpretations, one based on the analysis of the Perron-Frobenius spectrum and the other on that of dark states, of the

results presented in Section III concerning the optimal parameters ϕ_{opt} and τ_{opt} , as well as the presence of the threshold τ^* .

A. Perron-Frobenius analysis

Local monitoring repeatedly interrupts the unitary evolution of the system by projective measurements, resulting in an overall non-unitary evolution. The elementary step—a free evolution (4) for time τ followed by the detection attempt $\hat{D} = |\delta\rangle\langle\delta|$ —is governed by the (non-unitary) Perron-Frobenius operator¹

$$\begin{aligned}\hat{O}(\phi, \tau) &= [\mathbb{I} - \hat{D}]\hat{U}(\phi, \tau) \\ &= \sum_j \mu_j(\phi, \tau) |\mu_j(\phi, \tau)\rangle\langle\mu_j(\phi, \tau)|.\end{aligned}\quad (8)$$

The last equality represents the eigendecomposition of the operator, which depends on both ϕ and τ via the evolution generated by the Hamiltonian (1). Hereafter, we will omit the explicit dependence of eigenvalues and eigenvectors on these parameters for shortness. The Perron-Frobenius analysis allows us to characterize the asymptotic dynamics of the system in the long-time limit [46–49]. Repeatedly applying such operator on an initial state $|\psi_0\rangle$ generates a non-unitary evolution which does not preserve the probability. The *survival probability*

$$\begin{aligned}S(n) &= \sum_{i=0}^{N-1} |\langle i|\hat{O}^n(\tau)|\psi_0\rangle|^2 \\ &= \sum_{i=0}^{N-1} \sum_{j=0}^{N-1} |\mu_j|^{2n} |\langle i|\mu_j\rangle|^2 |\langle\mu_j|\psi_0\rangle|^2,\end{aligned}\quad (9)$$

is the probability that the detector has not clicked after n detection attempts, meaning that the walker has not been detected yet [38]. The survival probability relates to the detection probability (7) via $S(n) = 1 - P_{\text{det}}(n)$. The fact that $S(n) \leq 1$ means that $|\mu_j| \leq 1 \forall j$. In particular, the contributions from eigenvectors with $|\mu_j| < 1$ vanish for $n \rightarrow \infty$, while those from eigenvectors with $|\mu_j| = 1$ survive. The asymptotic dynamics is thus determined by the largest-modulus eigenvalues and their corresponding eigenvectors. The analysis of the eigenproblem of $\hat{O}(\phi, \tau)$ will equip us with the necessary tools to understand both the presence of the threshold τ^* and the optimal values of the parameters. For clarity of discussion, we focus here on the case of odd N , deferring the case of even N to Appendix B.

First, we focus on the existence of the threshold τ^* by studying how the Perron-Frobenius spectrum—evaluated at fixed N and $\phi = \phi_{\text{opt}}$ —differ depending on the regime

$\tau < \tau^*$ or $\tau > \tau^*$ [Fig. 4(a,b)]. For $0 < \tau < \tau^*$, all the eigenvalues fall within the unit circle, $|\mu_j| < 1 \forall j$ [see also the largest-modulus eigenvalue in Fig. 4(d)], meaning that all the modes decay and so the excitation will be transferred to the target state with unit probability in the long-time limit, $P_{\text{det}}(n \rightarrow \infty) = 1$. For $\tau > \tau^*$, instead, there may exist unit-modulus eigenvalues, indicating the emergence of modes which do not decay over time. This finding based on the analysis of the Perron-Frobenius spectrum aligns with the observations made in the previous sections, providing an estimate of τ^* that is consistent with the numerically observed one, $\tau^* \approx 1.55$. In turn, the value τ^* represents the upper bound to the interval between detection, over which maximizing the detection probability².

The optimal parameters, τ_{opt} and ϕ_{opt} , can be estimated by minimizing the Perron-Frobenius eigenvalue μ_{PF} with the largest modulus, which governs the asymptotic dynamics in the long-time limit. The study of $|\mu_{\text{PF}}|$ as a function of ϕ and τ in Fig. 4(c) reveals the following. At $\phi = \phi_{\text{opt}} = \pm\pi/2N$ (odd N), $|\mu_{\text{PF}}|$ decreases smoothly with increasing $\tau < \tau^*$, attains a minimum at τ_{opt} , and for $\tau > \tau^*$ its behavior becomes highly oscillatory, with $|\mu_{\text{PF}}| = 1$ for specific values of τ [Fig. 4(d)]. At a given measurement period $\tau < \tau^*$, $|\mu_{\text{PF}}|$ is minimum at the optimal phase ϕ_{opt} [Fig. 4(e)]. This behavior with respect to ϕ and τ is consistent with that of the detection probability in Fig. 2(b,d).

A remark is in order. The Perron-Frobenius analysis characterizes the asymptotic behavior in the long-time limit, whereas our previous investigation (Section III) assumes a finite observation time T , which may not correspond to the long-time limit (we will discuss it in Section IV C). In this regard, letting τ_{PF} be the value for which $|\mu_{\text{PF}}|$ is minimum, we observe that τ_{PF} is well approximated by τ_{opt} for low N , and this agreement extends to higher N upon increasing the total observation time T (data not shown).

These results show that the Perron-Frobenius analysis can be used to determine the optimal measurement period, provided the total observation time is large enough. As a final remark, we point out that τ_{PF} approaches the value $\pi/2$ as N increases, a behavior that we will explain in terms of dark states in the next Section IV B³.

B. Dark states

A complementary explanation of the optimal value of the measurement period can be provided using the con-

¹ The authors of Ref. [38] refer to this operator as the survival operator.

² Note that, regardless of τ , ϕ , and N (even or odd), we always observe the presence of a null eigenvalue with corresponding eigenstate $|\mu = 0\rangle = \hat{U}(\phi, -\tau)|\delta\rangle$, which trivially leads to $\hat{O}(\phi, \tau)|\mu = 0\rangle \equiv 0$.

³ Note that this trend is not captured by Fig. 3, where the maximum of the detection probability shifts instead toward lower τ , due the finite observation time T .

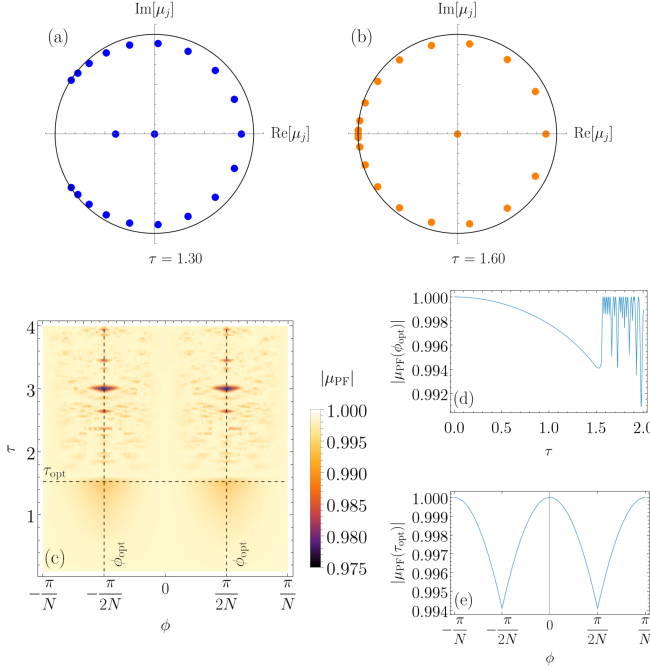


FIG. 4. Eigenvalues of the Perron-Frobenius operator (8) on the unit circle for two representative values of the sampling period, (a) $\tau < \tau^*$ and (b) $\tau > \tau^*$ at $\phi = \pi/2N$, $\delta = 10$. (c) Density plot of the largest-modulus PF eigenvalue $|\mu_{\text{PF}}|$ as a function of ϕ and τ . (d) Curve $|\mu_{\text{PF}}|$ as a function of τ at fixed $\phi = \pi/2N$. (e) Curve $|\mu_{\text{PF}}|$ as a function of ϕ at fixed $\tau = 1.53$. Other parameters are: $N = 21$, $\delta = 10$.

cept of *dark states*. As thoroughly explained in [38], the presence of a detector in a finite-dimensional quantum system, such as ours, splits the Hilbert space into two parts: a *bright subspace*, whose states are guaranteed to be eventually detected, ($P_{\text{det}}(\infty) = 1$), and a *dark subspace*, whose states are never detected, not even after an infinite number of detection attempts ($P_{\text{det}}(\infty) = 0$). A state that lies in the dark subspace is orthogonal (and remains orthogonal under the action of the evolution operator) to the detection site $|\delta\rangle$. A state that satisfies these properties—i.e., it is stationary with respect to the evolution and detection attempts—is called a *dark state*.

The total detection probability $P_{\text{det}}(\infty)$ is the squared modulus of the projection of the initial state $|\psi_0\rangle$ on the *bright space* [38]. Accordingly, whenever $|\psi_0\rangle$ has a nonzero projection on the *dark space*, then $P_{\text{det}}(\infty) < 1$, meaning that we are not guaranteed to detect the walker even with infinite measurements. Understanding when dark states arise and characterizing them is therefore important to optimize the detection probability.

Considering the time evolution in Eq. (4), a dark state can be built using the eigenvectors (2) of the Hamiltonian (1),

$$|\gamma_{n,m}\rangle = \sqrt{\frac{N}{2}} \left(\langle \delta | \lambda_n \rangle |\lambda_m\rangle - \langle \delta | \lambda_m \rangle |\lambda_n\rangle \right), \quad (10)$$

with $m \neq n$. Letting it evolve with $\hat{U}(\tau)$, we get the state

$$\hat{U}(\tau)|\gamma_{n,m}\rangle = \sqrt{\frac{N}{2}} e^{-i\lambda_m\tau} \left(\langle \delta | \lambda_n \rangle |\lambda_m\rangle - \langle \delta | \lambda_m \rangle e^{i(\lambda_m - \lambda_n)\tau} |\lambda_n\rangle \right), \quad (11)$$

which is orthogonal to the detection site $|\delta\rangle$ if

$$\lambda_m\tau \equiv \lambda_n\tau \pmod{2\pi}, \quad (12)$$

in which case the system never visits $|\delta\rangle$, resulting in $P_{\text{det}}(\infty) = 0$.

If no pairs of eigenvalues λ_m, λ_n satisfy the condition (12) and $\langle \lambda_j | \delta \rangle \neq 0 \forall j$, then the Hilbert space is *fully bright*, and there are no dark states [38]. Note that when Eq. (12) holds true, we have that $[\mathbb{I} - \hat{D}]\hat{U}(\tau)|\gamma_{n,m}\rangle = e^{-i\lambda_m\tau}|\gamma_{n,m}\rangle$, i.e. the Perron-Frobenius operator \hat{O} acts on dark states solely by multiplying them with a phase factor; that is, dark states are eigenstates of \hat{O} with eigenvalues of unit modulus. Moreover, they are the only possible eigenstates of modulus 1 of \hat{O} .⁴

In our model the condition $\langle \lambda_j | \delta \rangle \neq 0 \forall j$ is satisfied by any localized state $|\delta\rangle$ [see Eq. (2)], as our detection states, while the condition (12) can be satisfied in two ways:

(i) When the Hamiltonian's spectrum is degenerate, then Eq. (12) is satisfied $\forall \tau$ for each degenerate level. Degeneracies in the spectrum (3) arise only for $\phi = 0$ and $\phi = \pm\pi/N$, and the properties of the resulting dark states depend on the parity of N .

For even N , when $\phi = 0$ there exist $\frac{N}{2} - 1$ two-fold degenerate levels. In this case, all the stationary dark states constructed from the pairs of eigenstates in each degenerate level are orthogonal to the initial state. Therefore, they neither contribute to the dynamics of the system nor affect the detection probability. When $\phi = \pm\pi/N$ there exist $N/2$ two-fold degenerate levels. It can be proved (see Appendix B) that the initial state lies in the dark subspace spanned by the stationary dark states constructed from these degenerate levels. As a consequence, in this case the walker is never detected in $|\delta\rangle$, yielding to $P_{\text{det}}(\pm\pi/N) = 0$ in Fig. 2(a).

For odd N , calculations analogous to those in Appendix B reveal that for $\phi = 0, \pm\pi/N$ the total overlap

⁴ Indeed, since $\hat{U}(\tau)$ is a unitary operator, it preserves the norm. Therefore, for Perron-Frobenius operator to have an eigenvalue of modulus 1, it must be that $\hat{U}(\tau)|\mu\rangle$ (with $|\mu\rangle$ eigenstate corresponding to a unit modulus eigenvalue of \hat{O}) is orthogonal to $|\delta\rangle$. Otherwise, the action of $[\mathbb{I} - \hat{D}]$ would reduce its norm, making it impossible for the corresponding eigenvalue to have modulus 1. The only way \hat{O} can act on an eigenstate with eigenvalue of modulus 1 is via the time evolution operator followed by the identity. Consequently, such an eigenstate must be an eigenstate of the time evolution operator $\hat{U}(\tau)$ (which acts by multiplication with a phase) and simultaneously unaffected by $[\mathbb{I} - \hat{D}]$, meaning that the latter acts as the identity on it.

of the initial state with the dark space is $1/2$, thus explaining the minima of the detection probability for these values of ϕ in Fig. 2(b). For such values of ϕ , there exist $(N-1)/2$ two-fold degenerate levels, each contributing a dark state that, together, form the basis spanning the dark space.

(ii) Using any nondegenerate couple of eigenvalues $\lambda_m \neq \lambda_n$, there may exist proper combinations of τ and ϕ that lead to $\lambda_m \tau = \lambda_n \tau + 2k\pi$ for some $k \in \mathbb{Z}$. Plugging the eigenvalues (3) in the latter expression, i.e. Eq. (12), we derive the condition relating τ and ϕ under which dark states appear

$$\tau = \frac{k\pi}{2 \sin\left(\frac{\pi(m-n)}{N}\right) \sin\left(\phi - \frac{\pi(m+n)}{N}\right)}, \quad (13)$$

which establishes the lower bound $\tau \geq \pi/2$ for the presence of dark states arising from nondegenerate levels.

Such a lower bound is exactly attained for even N when $\phi = 0$. In all other cases, the τ at which the first dark state appears approaches $\pi/2$ as N grows. This is because the discrete arguments of the sine functions in Eq. (13) become denser in the interval $[0, 2\pi)$ for increasing N . For large N , it is therefore possible to find pairs (m, n) such that the product of the two sine functions, regardless of ϕ , is arbitrarily close to 1, implying the condition $\tau \gtrsim \pi/2$. In other words, for any ϕ the first dark state associated with nondegenerate levels will arise at $\tau \rightarrow \pi/2$ as $N \rightarrow \infty$, appearing as a dark-state line at $\tau \rightarrow \pi/2$ in the parameter space (ϕ, τ) . In general, for finite N , solutions to Eq. (13) constitute dark-state curves in the parameter space (ϕ, τ) , which correspond to low-detection-probability curves. Figures 2(a,b) represent a clear example: The detection probability in the parameter space (ϕ, τ) is low along the curves associated with the presence of dark states, including a nearly straight line at $\tau \gtrsim \pi/2$. In the region $\tau \geq \pi/2$, the dark-state curves become denser as N increases, because the number of dark states from nondegenerate levels is of order $O(N^2)$, and also as τ increases (see Appendix C).

To summarize, in the region $\tau < \pi/2$, for even N dark states at $\phi = 0$ do not affect the evolution of $|\psi_0\rangle$ yielding $P_{\text{det}}(\infty) = 1$, while for $\phi = \pm\pi/N$ the initial state is a dark state, yielding $P_{\text{det}}(\infty) = 0$; for odd N , the initial state has a finite overlap with dark states at $\phi = 0, \pm\pi/N$, yielding $P_{\text{det}}(\infty) = 1/2$. For $\phi \neq 0, \pm\pi/N$, the Hilbert space is fully bright in this region, so $P_{\text{det}}(\infty) = 1$ for both even and odd N . On the other hand, in the region $\tau \geq \pi/2$, the number of dark states increases as N and τ increase, yielding low-detection-probability curves in the parameter space (ϕ, τ) .

C. Asymptotic dynamics time scale

As pointed out in Section IV A, the Perron-Frobenius analysis provides useful insights into the asymptotic dy-

namics of the system. Related to our assumption of a finite observation time, this naturally leads to the question: What is the time scale over which such asymptotic behavior emerges? Such a time scale is governed by the spectral properties of the Perron-Frobenius operator (8), in particular by the spectral gap $\Delta \equiv 1 - |\mu_{\text{PF}}|$, where we recall μ_{PF} is the largest-modulus eigenvalue, according to which the asymptotic dynamics time scale can be estimated as $t_{\text{as}} \sim \Delta^{-1}$.

Because the Perron-Frobenius operator depends on the measurement period τ , the asymptotic time scale t_{as} varies with τ as well, as shown in Fig. 5(a). In the limit of small τ , t_{as} diverges due to the quantum Zeno effect, which prevents the walker from reaching—and thus being detected at—the measurement site. As τ increases, t_{as} monotonically decreases, reaching its minimum at τ_{opt} (minimum of $|\mu_{\text{PF}}|$), after which it quickly increases. Upon crossing the threshold τ^* , the system transitions to a regime characterized by a high sensitivity to small variations in the model parameters τ and ϕ [Fig. 2], a sensitivity also reflected in the values of t_{as} [Fig. 5(a)]. This behavior is consistent upon varying the number of sites N , with larger N leading to higher values of t_{as} . As anticipated at the end of Section IV A, the τ_{opt} that minimizes $|\mu_{\text{PF}}|$ approaches $\pi/2$ as N increases, a trend that is reflected in the corresponding behavior of the minimum of t_{as} in Fig. 5(a).

The asymptotic time at which the detection probability saturates increases as N increases. However, in practical cases, the experimentalist may be satisfied with the detection probability exceeding a certain threshold. This motivates the study in Fig. 5(b), where P_{det} is shown as a function of N and the total observation time T at τ_{opt} and ϕ_{opt} derived from the Perron-Frobenius analysis. First, we observe that the larger N , the larger T at which P_{det} saturates (i.e., $T \sim t_{\text{as}}$), and the larger the minimum T at which P_{det} is non-vanishing. Second, we note that the observation time T required to reach, e.g., $P_{\text{det}} \approx 80\%$ is almost an order of magnitude lower than that required to saturate. Third, we note that the observation time $T = 200$ considered in the present work is sufficiently long to observe the asymptotic dynamics and the saturation of P_{det} for $N < 21$, with $T \sim t_{\text{as}}$ at $N = 21$.

For larger N , the system takes longer to enter the asymptotic regime. Provided that the observation time satisfies $T \gtrsim t_{\text{as}}$, then P_{det} can saturate and the optimal sampling period τ_{opt} is identified by the minimum of $|\mu_{\text{PF}}|$. Instead, when $T < t_{\text{as}}$, the optimal sampling period τ_{opt} differs from that determined from the Perron-Frobenius analysis (minimum of $|\mu_{\text{PF}}|$), say $\tau_{\text{opt}}^{(\text{PF})}$, and it decreases with N at a rate that depends on T : the longer T , the slower the decrease, with τ_{opt} approaching $\tau_{\text{opt}}^{(\text{PF})}$ as $T \rightarrow \infty$ (data not shown).

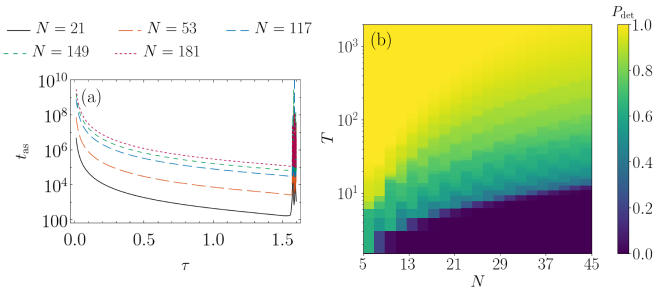


FIG. 5. (a) Asymptotic time t_{as} as a function of the sampling period τ for various odd N . (b) Density plot of P_{det} as a function of odd N and total observation time T , evaluated at the τ_{opt} corresponding to each N and at $\delta = (N - 1)/2$. In both panels the phase is fixed at $\phi_{opt} = \pi/2N$.

V. CONCLUSIONS

In this work, we have investigated the beneficial interplay between chirality and local monitoring in enhancing excitation transfer on a ring, within the framework of continuous-time quantum walks. Our findings address the gap in understanding how chirality, ϕ , and sampling period, τ , can be jointly optimized to overcome the limitations of purely unitary dynamics, usually stemming from destructive interference and presence of dark states. The resulting transfer protocol is optimal, significantly improving transfer probability, and robust, tolerating imperfect parameter tuning. This represents a substantial improvement over methods relying on precise fine-tuning, e.g., the evolution time in continuous-time quantum search [50], a common experimental challenge. Our approach in optimizing the transfer protocol leverages (i) a careful analysis of dark states to identify those, if any, relevant to the dynamics under investigation, and (ii) the Perron-Frobenius spectrum of the non-unitary dynamics to identify the optimal parameters, thus providing a general method for improving transport in monitored quantum systems.

Beyond deepening the fundamental understanding of first-detected-passage time problems and transport in closed loops, our results offer practical guidelines for designing quantum protocols that require robust and efficient state transfer [51], such as quantum routers [29]. Our study holds the potential to contribute to better design for quantum-walk-based computing [52] and for robust quantum search strategies [53].

Finally, hitting times are expected to directly impact the efficiency of quantum technologies, and the recent implementation of local monitoring on quantum hardware via mid-circuit measurements—either strong [41, 54] or weak [55]—highlights the experimental feasibility of such schemes. Furthermore, restart strategies are emerging as a further option to speed up quantum hitting times in monitored quantum systems [42, 56–58], offering potential insights for the understanding and design of efficient quantum algorithms.

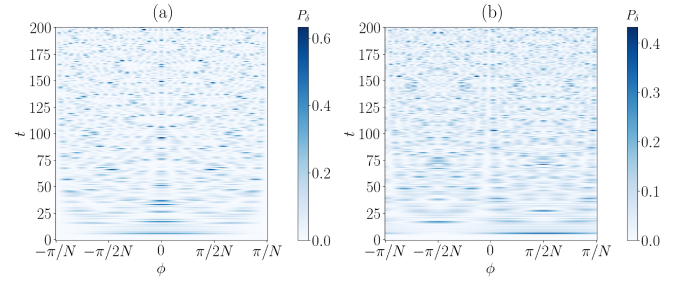


FIG. 6. Instantaneous transfer probability P_δ from site 0 to δ as a function of the phase ϕ and time t (a) for $N = 20$ and $\delta = N/2$ and (b) for $N = 21$ and $\delta = (N - 1)/2$.

ACKNOWLEDGMENTS

S.F., L.R., and G.B. acknowledge support by INFN through the project “QUANTUM”. S.F. and G.B. acknowledge support by Grant No. PNRR D. M. 118/2023. This work has been done under the auspices of GNFM-INdAM and M.G.A.P. acknowledges partial support by MUR and EU through the projects PRIN22-PNRR-P202222WBL-QWEST, and NQSTI-Spoke2-BaC QMORE (contract n. PE00000023-QMORE).

Appendix A: Purely-coherent transport under unitary evolution

As anticipated in the main text, the purely-coherent transport under unitary dynamics is not efficient. The instantaneous probability $P_\delta(\phi, t) = |\langle \delta | \hat{U}(\phi, t) | \psi_0 \rangle|^2$ typically remains low throughout the evolution, punctuated by narrow, sharp peaks. This is evident from the comparison between Figures 2 and 6: Fig. 6 shows P_δ as a function of the phase ϕ and time t , revealing that its values are consistently and significantly lower over the entire parameter range considered than those of the detection probability P_{det} in Fig. 2.

Appendix B: Perron-Frobenius analysis for even N

The Perron-Frobenius analysis in Section IV A focused on the case of odd N . Here we discuss the case of even N , which needs to be considered more carefully. The main differences between even and odd N root back to the degeneracies of the energy spectrum in Eq. (3). For odd N , all the energy levels but one—the highest ($j = 0$)—have a two-fold degeneracy when $\phi = 0$. These degeneracies are lifted when $\phi \neq 0$. For even N , instead, all the energy levels but two—the lowest ($j = N/2$) and the highest ($j = 0$)—have a two-fold degeneracy when $\phi = 0$. Nonzero phases lift these degeneracies except when $\phi = \pm\pi/N$, in which case all the energy levels, including the lowest and the highest, have a two-fold degeneracy. Following [38], we can construct a dark state

from each degenerate level λ_j as follows

$$|\gamma_j\rangle = \sqrt{\frac{N}{2}} \left(\langle \delta | \lambda_{j,2} \rangle | \lambda_{j,1} \rangle - \langle \delta | \lambda_{j,1} \rangle | \lambda_{j,2} \rangle \right). \quad (\text{B1})$$

For $\phi = 0$, the dark states read [38]

$$|\gamma_j\rangle = \sqrt{\frac{2}{N}} \sum_{k=0}^{N-1} \sin\left(\frac{2\pi j k}{N}\right) |k\rangle \quad (\text{B2})$$

with $j = 1, \dots, N/2 - 1$, and have no overlap with the initial state, $\langle 0 | \gamma_j \rangle = 0 \forall j$. As a result, these states do not contribute to the walker's dynamics and can be considered irrelevant in the evolution. These dark states are eigenstates of the Perron-Frobenius operator with unit-modulus eigenvalue [see Fig. 7(a,b)]. Consequently, the asymptotic dynamics relevant to excitation transfer will be governed by the subleading eigenvalue, defined as $\tilde{\mu}_{\text{PF}} \equiv \max_{|\mu_k| < 1} (\mu_k)$, i.e., the largest eigenvalue in modulus strictly less than one.

For $\phi = -\pi/N$, instead, the dark states read

$$|\gamma_j\rangle = \frac{1}{\sqrt{2N}} \sum_{k=0}^{N-1} \left(e^{i\frac{2\pi j k}{N}} + e^{-i\frac{2\pi(j+1)k}{N}} \right) |k\rangle \quad (\text{B3})$$

with $j = 0, \dots, N/2 - 1$, and always overlap with the initial state, $\langle 0 | \gamma_j \rangle = \sqrt{2/N} \forall j$. The initial state turns out to be completely dark for $\phi = -\pi/N$, as it is the equal superposition of all the $N/2$ dark states forming a basis for the dark subspace, $|0\rangle = \sqrt{2/N} \sum_{j=0}^{N/2-1} |\gamma_j\rangle$. The case $\phi = \pi/N$ can be treated analogously. Therefore, $P_{\text{det}}(n \rightarrow \infty) = 1$ if $\phi = 0$, and $P_{\text{det}}(n \rightarrow \infty) = 0$ if $\phi = \pm\pi/N$ [23].

The study of the largest-modulus Perron-Frobenius eigenvalue μ_{PF} is shown in Fig. 7(c). Similarly to the case of odd N , $|\mu_{\text{PF}}|$ smoothly attains a local minimum (which we identify as τ_{opt}) in the interval $\tau < \tau^*$, and then rapidly oscillates [Fig. 7(d)]. As for the dependence on the phase ϕ , μ_{PF} shows two minima at $\phi \neq 0$, in contrast with the optimal phase $\phi_{\text{opt}} = 0$ we expect for even N from the numerical optimization reported in the main text (Section III). On the other hand, as discussed above, dark states built using degenerate energy levels are irrelevant for excitation transfer at $\phi = 0$. At $\phi = 0$, one should thus consider the modulus of the subleading eigenvalue, $|\tilde{\mu}_{\text{PF}}|$ [red dot in Fig. 7(e)], which is lower than the two local minima of $|\mu_{\text{PF}}|$ when $\phi \neq 0$. We therefore conclude that the optimal phase for even N is $\phi = 0$.

Appendix C: Density of dark states increases with τ

In this Appendix, we prove that the density of dark states—i.e., the number of dark states in a certain interval $[\phi, \phi + \Delta\phi]$ at fixed τ —grows with τ in the region $\tau > \pi/2$. As discussed in Sec IV B, outside of

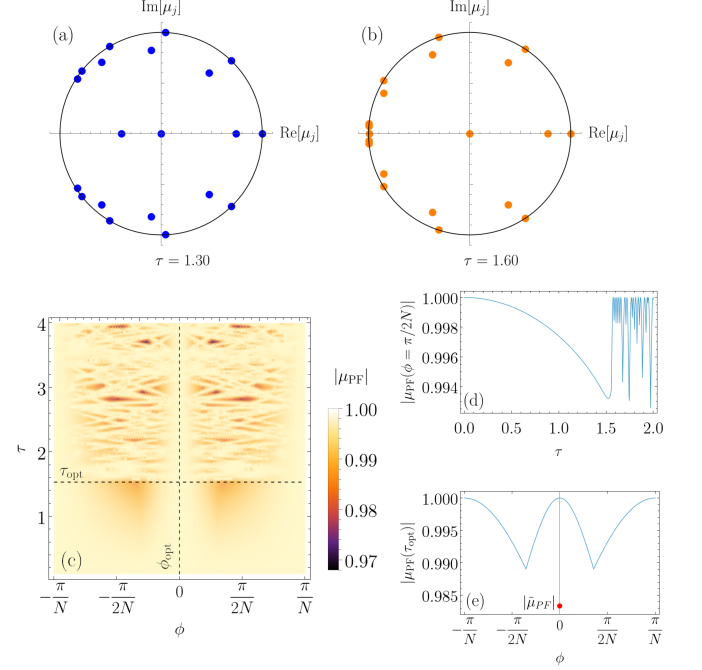


FIG. 7. Eigenvalues of the Perron-Frobenius operator (8) on the unit circle for two representative values of the sampling period, (a) $\tau < \tau^*$ and (b) $\tau > \tau^*$ at $\phi = 0$. (c) Density plot of the largest-modulus PF eigenvalue $|\mu_{\text{PF}}|$ as a function of ϕ and τ . (d) Curve $|\mu_{\text{PF}}|$ as a function of τ at fixed $\phi = \pi/2N$. (e) Curve $|\mu_{\text{PF}}|$ as a function of ϕ at fixed $\tau = 1.53$. The red circle denotes the subleading PF eigenvalue $|\tilde{\mu}_{\text{PF}}|$, which is the relevant one for the asymptotic dynamics at $\phi = 0$ (the initial state has zero overlap with dark states). Other parameters are: $N = 20$, $\delta = 10$.

the degenerate case, dark states correspond to solutions of Eq. (13). Graphically, these solutions are the intersections of two functions, $y_1 = k\pi$ and $y_2 = 2\tau \sin[\pi(m-n)/N] \sin[\phi - \pi(m+n)/N]$. On the plane (ϕ, y) , the function y_1 represents horizontal lines at integer multiples of π ; at fixed τ, m, n, N , the function y_2 is a sinusoidal function in ϕ , with τ acting as an amplification factor, provided that m, n satisfy $\sin[\pi(m-n)/N] \neq 0$. It is straightforward to see that the number of horizontal lines $y_1 = k\pi$ crossed by the function y_2 grows in any interval $[\phi, \phi + \Delta\phi]$ as τ increases, as was to be demonstrated. In other words, for larger values of τ , a finer tuning on ϕ is needed to avoid dark states, solutions of $y_1 = y_2$. Searching for a robust transfer protocol, this further motivates our choice of restricting to $\tau < \tau^*$.

- [1] S. E. Venegas-Andraca, Quantum walks: A comprehensive review, *Quantum Information Processing* **11**, 1015 (2012).
- [2] R. Portugal, *Quantum Walks and Search Algorithms*, 2nd ed. (Springer Cham, 2018).
- [3] J. P. Keating, N. Linden, J. C. F. Matthews, and A. Winter, Localization and its consequences for quantum walk algorithms and quantum communication, *Phys. Rev. A* **76**, 012315 (2007).
- [4] O. Mülken and A. Blumen, Continuous-time quantum walks: Models for coherent transport on complex networks, *Physics Reports* **502**, 37 (2011).
- [5] C.-M. Li, N. Lambert, Y.-N. Chen, G.-Y. Chen, and F. Nori, Witnessing quantum coherence: from solid-state to biological systems, *Scientific Reports* **2**, 885 (2012).
- [6] O. Mülken, V. Bierbaum, and A. Blumen, Coherent exciton transport in dendrimers and continuous-time quantum walks, *The Journal of Chemical Physics* **124**, 124905 (2006).
- [7] A. Olaya-Castro, C. F. Lee, F. F. Olsen, and N. F. Johnson, Efficiency of energy transfer in a light-harvesting system under quantum coherence, *Phys. Rev. B* **78**, 085115 (2008).
- [8] S. Lloyd, Quantum coherence in biological systems, *Journal of Physics: Conference Series* **302**, 012037 (2011).
- [9] S. Bose, Quantum communication through an unmodulated spin chain, *Phys. Rev. Lett.* **91**, 207901 (2003).
- [10] A. Rai, G. S. Agarwal, and J. H. H. Perk, Transport and quantum walk of nonclassical light in coupled waveguides, *Phys. Rev. A* **78**, 042304 (2008).
- [11] H. Tang, X.-F. Lin, Z. Feng, J.-Y. Chen, J. Gao, K. Sun, C.-Y. Wang, P.-C. Lai, X.-Y. Xu, Y. Wang, L.-F. Qiao, A.-L. Yang, and X.-M. Jin, Experimental two-dimensional quantum walk on a photonic chip, *Science Advances* **4**, eaat3174 (2018).
- [12] M. Mohseni, P. Rebentrost, S. Lloyd, and A. Aspuru-Guzik, Environment-assisted quantum walks in photosynthetic energy transfer, *The Journal of Chemical Physics* **129**, 174106 (2008).
- [13] M. B. Plenio and S. F. Huelga, Dephasing-assisted transport: quantum networks and biomolecules, *New Journal of Physics* **10**, 113019 (2008).
- [14] P. Rebentrost, M. Mohseni, I. Kassal, S. Lloyd, and A. Aspuru-Guzik, Environment-assisted quantum transport, *New Journal of Physics* **11**, 033003 (2009).
- [15] C. Maier, T. Brydges, P. Jurcevic, N. Trautmann, C. Hempel, B. P. Lanyon, P. Hauke, R. Blatt, and C. F. Roos, Environment-assisted quantum transport in a 10-qubit network, *Phys. Rev. Lett.* **122**, 050501 (2019).
- [16] S. Huelga and M. P. and, Vibrations, quanta and biology, *Contemporary Physics* **54**, 181 (2013).
- [17] F. Caruso, A. W. Chin, A. Datta, S. F. Huelga, and M. B. Plenio, Highly efficient energy excitation transfer in light-harvesting complexes: The fundamental role of noise-assisted transport, *The Journal of Chemical Physics* **131**, 105106 (2009).
- [18] E. Zerah-Harush and Y. Dubi, Universal origin for environment-assisted quantum transport in exciton transfer networks, *The Journal of Physical Chemistry Letters* **9**, 1689 (2018).
- [19] M. Varbanov, H. Krovi, and T. A. Brun, Hitting time for the continuous quantum walk, *Phys. Rev. A* **78**, 022324 (2008).
- [20] L. Razzoli, M. G. A. Paris, and P. Bordone, Transport efficiency of continuous-time quantum walks on graphs, *Entropy* **23**, 85 (2021).
- [21] L. Novo, S. Chakraborty, M. Mohseni, H. Neven, and Y. Omar, Systematic dimensionality reduction for quantum walks: Optimal spatial search and transport on non-regular graphs, *Scientific Reports* **5**, 13304 (2015).
- [22] S. Cavazzoni, L. Razzoli, P. Bordone, and M. G. A. Paris, Perturbed graphs achieve unit transport efficiency without environmental noise, *Phys. Rev. E* **106**, 024118 (2022).
- [23] Z. Zimborás, M. Faccin, Z. Kádár, J. D. Whitfield, B. P. Lanyon, and J. Biamonte, Quantum transport enhancement by time-reversal symmetry breaking, *Scientific Reports* **3**, 2361 (2013).
- [24] D. Lu, J. D. Biamonte, J. Li, H. Li, T. H. Johnson, V. Bergholm, M. Faccin, Z. Zimborás, R. Laflamme, J. Baugh, and S. Lloyd, Chiral quantum walks, *Phys. Rev. A* **93**, 042302 (2016).
- [25] M. Frigerio, C. Benedetti, S. Olivares, and M. G. A. Paris, Generalized quantum-classical correspondence for random walks on graphs, *Phys. Rev. A* **104**, L030201 (2021).
- [26] M. Frigerio, C. Benedetti, S. Olivares, and M. G. A. Paris, Quantum-classical distance as a tool to design optimal chiral quantum walks, *Phys. Rev. A* **105**, 032425 (2022).
- [27] E. Annoni, M. Frigerio, and M. G. A. Paris, Enhanced quantum transport in chiral quantum walks, *Quantum Information Processing* **23**, 117 (2024).
- [28] A. Sett, H. Pan, P. E. Falloon, and J. B. Wang, Zero transfer in continuous-time quantum walks, *Quantum Information Processing* **18**, 159 (2019).
- [29] A. Bottarelli, M. Frigerio, and M. G. A. Paris, Quantum routing of information using chiral quantum walks, *AVS Quantum Science* **5**, 025001 (2023).
- [30] G. Ragazzi, S. Cavazzoni, C. Benedetti, P. Bordone, and M. G. A. Paris, Scalable structure for chiral quantum routing, *Entropy* **27**, 498 (2025).
- [31] S. Redner, *A Guide to First-Passage Processes* (Cambridge University Press, 2001).
- [32] A. J. Bray, S. N. Majumdar, and G. S. and, Persistence and first-passage properties in nonequilibrium systems, *Advances in Physics* **62**, 225 (2013).
- [33] O. Bénichou and R. Voituriez, From first-passage times of random walks in confinement to geometry-controlled kinetics, *Physics Reports* **539**, 225 (2014).
- [34] R. Metzler, G. Oshanin, and S. Redner, eds., *First Passage Phenomena and Their Applications* (World Scientific, Singapore, 2014).
- [35] S. Dhar, S. Dasgupta, and A. Dhar, Quantum time of arrival distribution in a simple lattice model, *Journal of Physics A: Mathematical and Theoretical* **48**, 115304 (2015).
- [36] S. Dhar, S. Dasgupta, A. Dhar, and D. Sen, Detection of a quantum particle on a lattice under repeated projective measurements, *Phys. Rev. A* **91**, 062115 (2015).

- [37] H. Friedman, D. A. Kessler, and E. Barkai, Quantum walks: The first detected passage time problem, *Phys. Rev. E* **95**, 032141 (2017).
- [38] F. Thiel, I. Muallem, D. Meidan, E. Barkai, and D. A. Kessler, Dark states of quantum search cause imperfect detection, *Phys. Rev. Res.* **2**, 043107 (2020).
- [39] M. J. Kewming, A. Kiely, S. Campbell, and G. T. Landi, First passage times for continuous quantum measurement currents, *Phys. Rev. A* **109**, L050202 (2024).
- [40] F. A. Grünbaum, L. Velázquez, A. H. Werner, and R. F. Werner, Recurrence for discrete time unitary evolutions, *Communications in Mathematical Physics* **320**, 543 (2013).
- [41] Q. Wang, S. Ren, R. Yin, K. Ziegler, E. Barkai, and S. Tornow, First hitting times on a quantum computer: Tracking vs. local monitoring, topological effects, and dark states, *Entropy* **26**, 869 (2024).
- [42] R. Yin, Q. Wang, S. Tornow, and E. Barkai, Resonances of recurrence time of monitored quantum walks, *The Journal of Chemical Physics* **162**, 244114 (2025).
- [43] N. Byers and C. N. Yang, Theoretical considerations concerning quantized magnetic flux in superconducting cylinders, *Phys. Rev. Lett.* **7**, 46 (1961).
- [44] P. Facchi and S. Pascazio, Quantum Zeno dynamics: mathematical and physical aspects, *Journal of Physics A: Mathematical and Theoretical* **41**, 493001 (2008).
- [45] I. Georgescu, Quantum zeno effect at 45, *Nature Reviews Physics* **4**, 289 (2022).
- [46] P. Gaspard, *Chaos, Scattering and Statistical Mechanics*, Cambridge Nonlinear Science Series (Cambridge University Press, 1998).
- [47] M. Khodas, S. Fishman, and O. Agam, Relaxation to the invariant density for the kicked rotor, *Phys. Rev. E* **62**, 4769 (2000).
- [48] I. García-Mata, M. Saraceno, and M. E. Spina, Classical decays in decoherent quantum maps, *Phys. Rev. Lett.* **91**, 064101 (2003).
- [49] D. Chruściński, S. Denisov, W. Tarnowski, and K. Życzkowski, Spectral delineation of markov generators: Classical vs quantum (2025), [arXiv:2504.07903 \[cond-mat.stat-mech\]](#).
- [50] A. M. Childs and J. Goldstone, Spatial search by quantum walk, *Phys. Rev. A* **70**, 022314 (2004).
- [51] A. Kay, Perfect, efficient, state transfer and its application as a constructive tool, *International Journal of Quantum Information* **08**, 641 (2010).
- [52] X. Qiang, S. Ma, and H. Song, Quantum walk computing: Theory, implementation, and application, *Intelligent Computing* **3**, 0097 (2024).
- [53] A. M. Childs, E. Deotto, E. Farhi, J. Goldstone, S. Gutmann, and A. J. Landahl, Quantum search by measurement, *Phys. Rev. A* **66**, 032314 (2002).
- [54] S. Tornow and K. Ziegler, Measurement-induced quantum walks on an IBM quantum computer, *Phys. Rev. Res.* **5**, 033089 (2023).
- [55] T. Heine, E. Barkai, K. Ziegler, and S. Tornow, Quantum walks: First hitting times with weak measurements (2025), [arXiv:2506.21168 \[quant-ph\]](#).
- [56] R. Yin and E. Barkai, Restart expedites quantum walk hitting times, *Phys. Rev. Lett.* **130**, 050802 (2023).
- [57] S. Roy, S. Gupta, and G. Morigi, Causality, localisation, and universality of monitored quantum walks with long-range hopping (2025), [arXiv:2504.12053 \[quant-ph\]](#).
- [58] R. Yin, Q. Wang, S. Tornow, and E. Barkai, Restart uncertainty relation for monitored quantum dynamics, *Proceedings of the National Academy of Sciences* **122**, e2402912121 (2025).